EVALUATING DIFFERENT SCALES OF REMOTELY SENSED DATA TO PREDICT AMPHIBIAN HABITAT DISTRIBUTIONS

Jeremy P. Shive and Charles R. Peterson
Department of Biological Sciences
Idaho State University
Pocatello, ID 83209-8130
(e-mail: shivejere@isu.edu, petechar@isu.edu)

ABSTRACT
We evaluated three scales (spatial and spectral) of remotely sensed data to model wetland habitat distributions in two ecologically distinct wilderness landscapes. Two multispectral datasets, Landsat ETM+ (30 m, 6 bands) and ADAR 5500 (2 m, 4 bands), and one hyperspectral dataset, Hymap (3.5-4 m, 126 bands), were processed using numerous classification algorithms to map wetland features. The classifications were validated using traditional error matrices and also interpreted from the viewpoint of an ecologist conducting field surveys. The HyMap hyperspectral data produced the greatest classification accuracies of fine-scale wetland features; it was unmatched by the multispectral data. The hyperspectral data provide additional information used to distinguish habitat features and should be considered a valuable tool for future inventory and monitoring initiatives that require fine-scale comprehensive information across large spatial extents.

Keywords: hyperspectral, inventory and monitoring, scale, Frank Church-River of No Return Wilderness.

INTRODUCTION

Based on observations over the past two decades it has been recognized that amphibian populations are exhibiting global population declines, which has stimulated concern among herpetologists and conservation biologists around the world. In response to ongoing population declines, substantial effort has been invested in establishing broad scale inventory and monitoring initiatives to better understand current amphibian population distributions and relative abundance across large landscapes.

In most cases, inventory and monitoring programs have only recently begun and the collection of initial inventory data remains the primary objective. Following the inventory phase, repeated surveys can form the basis for a monitoring program. Monitoring specific key amphibian habitat features (e.g., shallow shorelines and emergent vegetation) can serve as a surrogate for organismal response to habitat alteration over time. Modeling habitat features may also provide insights concerning the effects of proposed management actions on population dynamics across broad spatial scales.

The ideal scenario for an inventory and monitoring program would be a comprehensive survey of all habitat available within the study area (Fellers 1997), but this is rarely possible because current amphibian habitat distribution is commonly unknown. Small wetland sites (i.e., several m^2) are not commonly detected using traditional methods of environmental mapping, such as USGS topographic maps and Digital Orthophoto Quarter Quadrangle (DOQQ) aerial photographs. Standard imagery or maps typically help identify potential habitat distribution and assist a researcher in designing the most appropriate sampling scheme or site selection process. Since these data sources do not always provide accurate information, ground based surveys are hindered due to the total number of hours needed to thoroughly inventory a region such as a forest or wilderness area.

Recent advances in remote sensing technologies and the numerous scale options (i.e., radiometric, spatial, and spectral) commercially available today significantly enhance researchers' abilities to design studies and investigate biological or ecological questions that previously could not be considered. In this study, we have taken a multi-scale approach to assess the applicability of current remote sensing technologies to model wetland habitat distribution in a wilderness area. The results are interpreted from an inventory and monitoring application perspective to propose the most appropriate remotely sensed data type for future broad scale amphibian conservation programs.

Study Area

The study area is located in the Frank Church-River of No Return Wilderness, Idaho (Figure 1). Two ecologically different landscapes within the study area were chosen as representative study sites. The first site is located along Big Creek, a fourth-order stream and major tributary to the Middle Fork of the Salmon River with elevations ranging from approximately 1100 m to 1900 m. Douglas Fir (*Pseudotsuga menziesii*) and Ponderosa Pine (*Pinus ponderosa*) are the dominant tree species within the drainage while Black

Cottonwood (*Populus balsamifera*), Water Birch (*Betula occidentalis*), and Green Alder (*Alnus viridis*) represent the tree species most commonly found in the riparian areas along Big Creek and local tributaries. Rocky Mountain Maple (*Acer glabrum*), Syringa (*Philadelphus lewisii*), and Prairie Rose (*Rosa woodsii*) comprise the majority of understory shrubs in the riparian area, while Giant Wildrye (*Elymus piperi*) and Idaho Fescue (*Festuca spp*.) characterize the drier upland hillsides. The second site is located in the Bighorn Crags, a sub-alpine region of the wilderness characterized by high elevation glaciated cirque basins with elevations ranging from approximately 2400 m to 2900 m. Sub Alpine Fir (*Abies lasiocarpa*), Engelmann Spruce (*Picea engelmanni*), and Whitebark Pine (*Pinus albicaulis*) characterize the forested uplands and valley floors. Beargrass (*Xerophyllum tenax*) and Grouse Whortleberry (*Vaccinium scoparium*) dominate the forest understory and sedge (*Carex spp*.) is commonly associated with mesic meadows and wetland habitat.

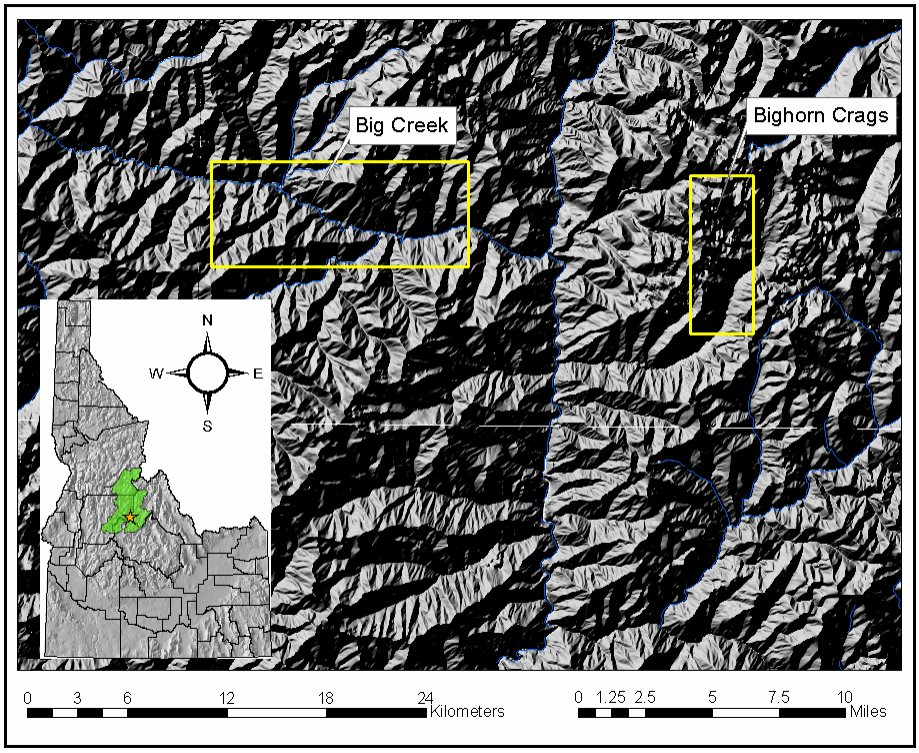

Figure 1. The location of the Frank Church-River of No Return Wilderness, Idaho shown in green, with the study area denoted by the orange star. The approximate area of the study sites are delineated by the yellow border.

METHODS

Image Acquisitions and Processing

We performed all image processing and image classifications using Research Systems Inc.'s ENVI® 3.5 (RSI, 2002) and all GIS analyses were conducted using Environmental Systems Research Institute, Inc.® ArcGIS 8.2.

Multispectral Data

The first multispectral dataset was collected on July 10, 2002 by NASA's Landsat 7 Enhanced Thematic Mapper Plus (ETM+) satellite. Landsat ETM+ uses an oscillating scanning mirror with +/- 5.78º angular displacement off-nadir, resulting in an image swath of approximately 185 km and an instantaneous field of view (IFOV) (i.e., spatial resolution) of 30 m for all spectral bands. The Landsat ETM+ sensor collects six spectral bands of 8-bit data in the visible and infrared region of the electromagnetic (EM) spectrum (Table 1).

The Landsat ETM+ data were received in the form of digital number (DN) values and we converted these data to at-sensor reflectance. The reflectance conversion process is calculated as:

$$L_\lambda = ((LMAX - LMIN)/255) \cdot DN + LMIN$$

Where, L_λ, is radiance ($W/m^2/sr/\mu m$) for each spectral band, LMIN and LMAX are the gains and bias information respectively that are obtained from the image header file, and DN represents the assigned digital number of a spectral band.

Reflectance, ρ_λ, for each band is calculated as:

$$\rho_\lambda = \frac{\pi \cdot L_\lambda}{ESUN_\lambda \cdot \cos\theta \cdot d_r}$$

Where L_λ is the radiance for each spectral band, $ESUN_\lambda$ is the mean exo-atmosphere irradiance for each band (Landsat 7 Science Users Handbook, Chapter 11, 2002) in units of $W/m^2/\mu m$, cosine θ ($\theta = 90^\circ - \beta$) where β is the sun elevation angle. The term d_r is defined as $1/d_{e\text{-}s}^2$ where $d_{e\text{-}s}$ is the relative distance between the earth and sun in astronomical units (Duffie and Beckman 1980). The term d_r is calculated as:

$$d_r = 1 + 0.033 \cos(DOY\ 2\pi/365)$$

Where DOY is the sequential day of year.

The second multispectral dataset was collected on July 31, 2002 by Positive System's Airborne Data Acquisition and Registration (ADAR) 5500 system. The ADAR 5500 system incorporates Kodak Professional DCS 420 digital frame cameras with a 39º across-track field of view and a 0.44 mrad instantaneous field of view (IFOV) for each pixel in the CCD array. The ADAR 5500 was configured to collect four spectral bands of 8-bit data in the visible and near-infrared regions of the EM spectrum (Table 1) with a spatial resolution of approximately 2 m.

Hyperspectral Data

Hyperspectral data were acquired on June 30, 2002 by the airborne hyperspectral sensor HyMap (Cocks et al. 1998). HyMap uses a whiskbroom sensor with a 61.3º field of view (512 across track pixels) with an IFOV of 2.5 mrad along track and 2.0 mrad across track. HyMap is typically flown on a twin engine fixed wing Cessna mounted with a gyro-stabilized platform and incorporates a Boeing C-MIGITS II Global Positioning System (GPS)/Inertial Monitoring Unit (IMU) that corrects for aircraft roll, pitch, and yaw caused by turbulence. HyMap collects 128 spectral bands of 12-bit data covering 0.44 μm – 2.5 μm spectral region with a 15 nm average bandwidth (Table 1). Spatial resolution of the hyperspectral data collected over the Big Creek and Bighorn Crags study sites were 4 m and 3.5 m respectively.

The raw radiance data ($\mu W/cm^2$ /sr/nm) collected by the HyMap sensor are influenced by incoming solar irradiance and atmospheric absorptions from gases such as water vapor, ozone, carbon monoxide, oxygen, carbon dioxide, nitrous oxide, and methane (Gao et al. 1993). In order to produce spectral signatures that can be compared with laboratory or ground-based spectra, and quantitatively evaluated, the radiance data must be converted into apparent reflectance. The data vendor provided the hyperspectral imagery already atmospherically corrected using a radiative transfer model ATREM (Gao et al. 1997). The reflectance data were also spectrally "polished" using the Empirical Flat Field Optimal Reflectance Transformation (EFFORT), which removes residual and cumulative calibration and model imposed errors (Boardman 1998a).

The Hymap data are collected on a pixel-by-pixel basis and therefore geometric corrections must be made to the data to insure that each pixel can be referenced to a real-world coordinate system and used with other spatial datasets. All of the pixel coordinates recorded during the flight are organized into an Input Geometry File (IGM) that preserves the spatial integrity of the ground pixel relationships (Boardman 1999). Then a Geometry Lookup Table (GLT) is created which provides the truly measured coordinate positions supplied from the onboard C-MIGITS II GPS/IMU that corrects for platform motion and topography (Boardman 1999). We applied the geometric correction files to the reflectance data which eliminated overlapping redundant pixels and resampled "gaps" in the data producing a geometrically corrected contiguous image.

We used the Minimum Noise Fraction (MNF) transform to segregate the noise dominated spectral bands from the "information rich" spectral bands, and to spectrally reduce the computationally expensive dataset. The MNF transform can be considered a two-step principal components analysis that accounts for correlated noise in the data caused by contiguous sequential spectral bands. The first step calculates a noise covariance matrix and decorrelates and rescales the noise in the data (Green et al. 1988). The second step is a standard Principal Component (PC) transformation where the transformed spectral bands are organized by decreasing variance (Green et al. 1988). We examined the MNF transformed images using ENVI's animation feature and considered the resulting eigenvalue plots to determine the dimensionality of each dataset. The assigned image

dimensionality (i.e., the significant MNF bands) served as the input for subsequent hyperspectral processing steps.

We used the Pixel Purity Index (PPI) and n-Dimensional Visualizer (nDV) to spatially reduce the dataset and identify the most spectrally "pure" pixels, or endmembers, in the imagery. The PPI repeatedly projects n-dimensional scatter plots onto a random unit vector cumulatively scoring the pixels with the highest and lowest values as well as any other pixels falling within a defined standard deviation. Pixels with extreme values are scored most often and theoretically represent the corners, or potential endmembers, of the multi-dimensional cloud of image pixels (Boardman 1993). The nDV rotates potential endmember pixels (i.e., the results from the PPI) in a user-defined number of spectral dimensions. We altered the number of spectral dimensions to expose endmember "corners" that are less evident in some collapsed dimensional axes. We selectively chose the most spatially distinct corners in the multidimensional cloud of data and exported each endmember pixel(s). This tool is interactively linked to the image and through repetitive investigations of the spatial distributions of endmember pixels, we were able to select image endmembers located within boundaries of features of interest (e.g., wetlands).

Image Classification

Multispectral Data

The intent of the classification process is to map the distribution of wetland habitat as an indicator of potential amphibian habitat. We are not abiding to a strict definition of a wetland and from this point forward we will refer to a wetland site generically as any location of standing water in the form of permanent lakes or ephemeral ponds and pools, but also wet meadows where water presence may be no more than a thin film or moist soil holding small puddles. These site descriptions characterize typical amphibian habitat in the study area and hence are the focus of our classification efforts.

The topography throughout the study area is characterized by steep slopes and ridges that produce an abundance of shadow influenced locations within both study sites. Shadows and water exhibit a similar spectral response pattern of very low reflectance, and consequently these two classes were continually misclassified and confused in the multispectral imagery. We decided the most accurate classifications of water features (i.e., wetlands) would be to distinguish them from the shadowed pixels in each image, and we paid close attention to selecting representative water and shadow training ROI's (Regions of Interest). We selected pixels in multiple training sites across the extent of each dataset to develop statistically representative ROI's needed for appropriate image classifications (Jensen 2000). We were not concerned with the ability to correctly classify surrounding vegetation features and collapsed all other image features into a single class labeled "everything else". This approach delineates a total of three spectral training ROI classes (i.e., water, shadow, and everything else) used to classify the Landsat ETM+ imagery. We attempted to classify an additional feature, sedge, in the ADAR 5500 imagery, but following preliminary visual assessment we determined the

Table 1. A comparison of the remotely sensed data specifications used in the study.

Sensor	Type of Imagery	Spatial Resolution	Spatial Extent*	Spectral Bands	Spectral Sampling	Spectral Range	Radiometric Resolution
HyMap	Hyperspectral	3.5 - 4m	2.5km x 20km	126	VIS 15nm	450nm - 890nm	12 bit
					NIR 15nm	890nm - 1350nm	
					SWIR1 13nm	1400nm - 1800nm	
					SWIR2 17nm	1950nm - 2480nm	
ADAR 5500	Multispectral	2m	2km x 3km (per frame)	4	Band 1(Blue)	460nm - 550nm	8 bit
					Band 2 (Green)	520nm - 610nm	
					Band 3 (Red)	610nm - 700nm	
					Band 4 (Near Infrared)	780nm - 920nm	
Landsat ETM+	Multispectral	30m	185km x 185km	6	Band 1 (Blue)	450nm - 515nm	8 bit
					Band 2 (Green)	525nm - 605nm	
					Band 3 (Red)	630nm - 690nm	
					Band 4 (Near Infrared)	750nm - 900nm	
					Band 5 (Infrared)	1550nm - 1750nm	
					Band 7 (Infrared)	2080nm - 2350nm	

* Estimates are approximate spatial extent; after georeferencing spatial extent may be reduced slightly due to topography

results were below an acceptable level of accuracy. This resulted in a total of three training ROI classes (i.e., water, shadow, and everything else) considered to classify the ADAR 5500 data.

We ran the Jeffries-Matusita ROI separability measure to quantitatively evaluate the statistical separability of the training ROI classes used for the multispectral image classifications (Richards 1999)(Table 2). The output separability values range from 0-2, with values falling below 1 suggesting poor or unacceptable separability and values above 1.9 indicating the classes have good separability (Richards 1999).

Table 2. Jeffries-Matusita ROI separability results for the multispectral training classes.

	Landsat ETM+		ADAR 5500	
	Big Creek	**Bighorn Crags**	**Big Creek**	**Bighorn Crags**
	Water	Water	Water	Water
Shadow	1.991	1.948	1.915	1.721
Everything Else	1.985	1.999	1.97	1.991

Big Creek Study Site
We used the Spectral Angle Mapper (SAM) classification algorithm for both the Landsat ETM+ and ADAR 5500 datasets at the Big Creek study site. The SAM classification algorithm determines the similarity between image spectra and training ROI spectra based on the angle between them calculated as a vector in n-dimensional space, where "n" equals the number of input bands or dimensionality (Kruse et al. 1993). Smaller angles represent better matches to ROI reference spectra. We adjusted the maximum allowable angle across a range starting at 0.1 radians up to 3.0 radians to determine the best acceptable angular tolerance. This algorithm is relatively insensitive to changes in scene illumination and albedo effects (Kruse et al. 1993), which may have contributed to the success of this approach applied to a landscape that is highly influenced by drastic changes in image brightness caused by topography and shadows.

Bighorn Crags Study Site
Following numerous attempts to apply traditional supervised classification algorithms to the Landsat ETM+ data in the Bighorn Crags study area, we concluded that the best approach was using a 2-D scatter plot incorporating two near-infrared spectral bands (i.e., Band 4 vs. Band 5). Water exhibits very low spectral response patterns in the near-infrared region of the EM spectrum and would expectedly be located near the lowest spectral values on both axis of the scatter plot. By exploiting this known spectral feature characteristic, we subjectively selected and iteratively refined a group of pixels located in the lower left corner of the 2-D scatter plot (Figure 2). We exported the selected pixels as ROI's and produced a "standing water" classification image.

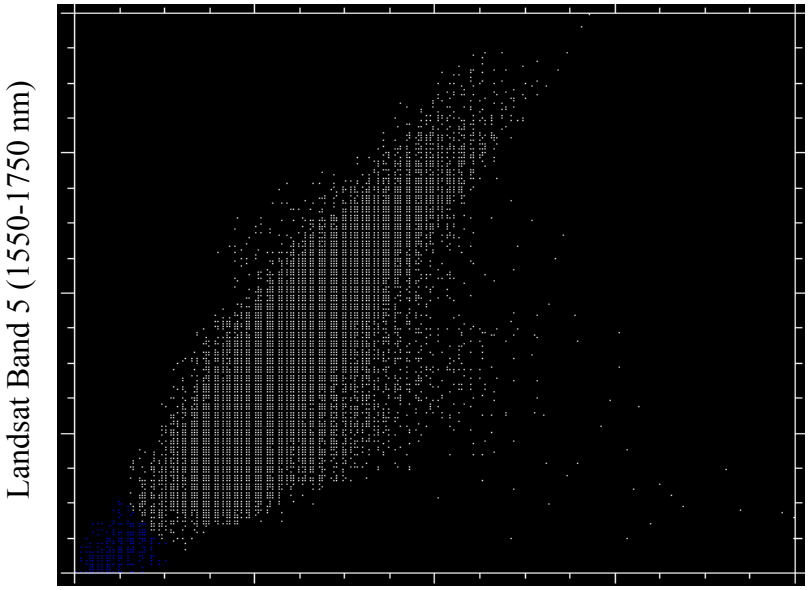

Figure 2. 2-D scatter plot used to create the Landsat ETM+ standing water classification map of the Bighorn Crags study site.

We used the Maximum Likelihood algorithm to classify the ADAR 5500 data. The Maximum Likelihood algorithm considers both spectral variance, plotted as a mean vector, and covariance of the training ROI's (Jensen 2000). The underlying assumption of this algorithm is a Gaussian distribution, which is a reasonable assumption for common spectral classes such as water (Jensen 2000). Based on the spectral response pattern and associated statistics of the ROI training classes, a probability density function is created that assesses the individual probability for each image pixel. We designated a probability threshold for each ROI training class determined through repetitive classification attempts, and any pixel falling within the designated threshold range is assigned to the corresponding ROI class.

Hyperspectral Data

Given the unique attributes of hyperspectral data, such as the ability to map endmember sub-pixel fractional abundances, we tested the Mixture Tuned Matched Filter (MTMF) classification algorithm (Boardman 1998b). Initially we ran MTMF on all image endmembers identified through the PPI and nDV image processing steps. We also experimented with traditional supervised classification algorithms in attempt to produce the most accurate wetland classifications.

Big Creek Study Site

Given the increased spectral resolution and range of the hyperspectral dataset, we were able to identify much finer-scale wetland habitat features than water alone. We identified Standing Water and Sediment (SWS) and Shallow Stream Water (SSW) image endmembers (Figure 3). We used these endmembers to classify wetland habitats associated with floodplain and stream features such as side-channels and backwater

pools. We also identified a wet meadow (WM) endmember representative of a mixture of sedges and grasses directly associated with water presence (Figure 4).

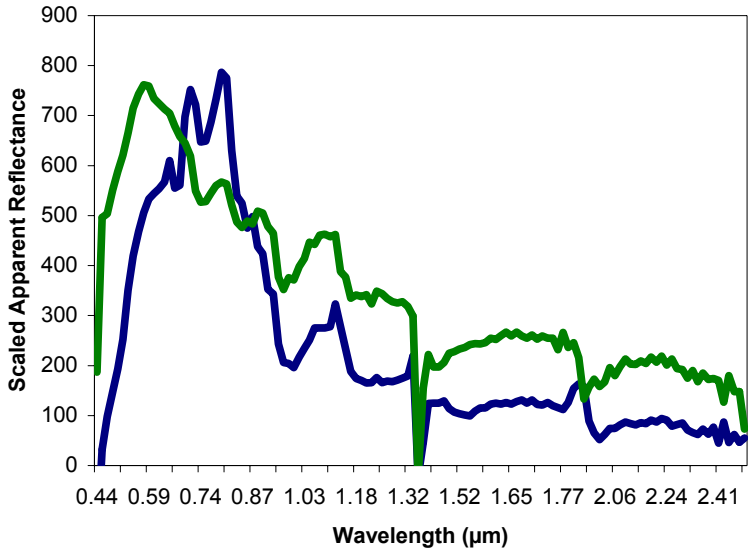

Figure 3. Shallow Water Sediment (SWS, shown in blue) and Shallow Stream Water (SSW, shown in green) endmember spectral profiles.

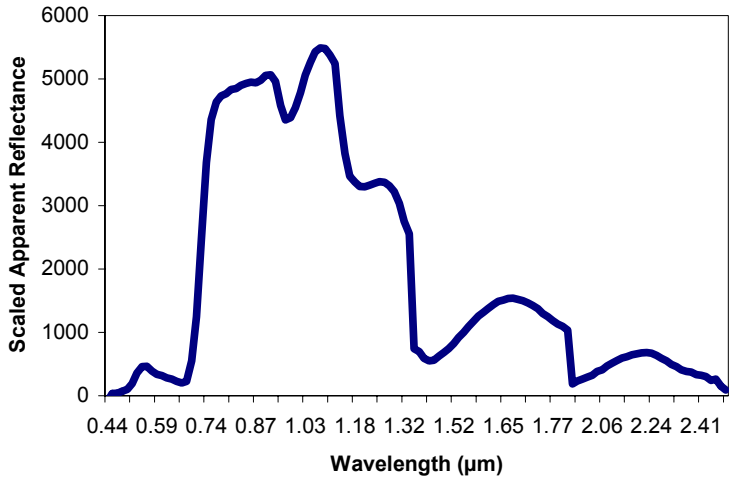

Figure 4. Wet Meadow (WM) endmember spectral profile.

We used the SAM algorithm to classify the SWS and SSW endmembers. We believe that the characteristics of the SAM algorithm (i.e., insensitivity to changes in illumination and albedo) contributed to the classification success for these features that commonly exhibit variable reflectance patterns due to surface turbulence of flowing water. We experimented with the same angular ranges described above for the multispectral

datasets, to assign the angle that produced the most accurate classifications while minimizing omission and commission errors.

We used the MTMF algorithm to produce a classification of sub-pixel fractional abundances for the wet meadow endmember. Although the goal was not to quantify the accuracy of fractional abundance value, this classification algorithm is potentially the best approach to identify small wetland features common to this study area. MTMF builds upon the strengths of both matched filtering and spectral unmixing algorithms while avoiding the disadvantages of both (Boardman 1998b). Matched filtering performs partial spectral unmixing and identifies the fractional abundance of a spectral endmember on a continuous scale without knowing all of the background endmember signatures (Harsanyi and Chang 1994, Boardman et al. 1995). Spectral unmixing takes advantage of the hyperspectral leverage (i.e., an overdetermined solution caused by a greater number of spectral bands than unknowns) to solve the linear mixed pixel problem (Boardman 1993). The combined strengths of these two algorithms provide a unique and robust method to map endmember fractional abundances.

MTMF results in two image outputs, the first being a Matched Filter (MF) image and the second an Infeasibility image. The best classification accuracies required the useful contribution of information from both resulting images combined into a single feature classification. We loaded the MF and Infeasibility images as the axes of a 2-D scatter plot diagram and subjectively selected, and iteratively refined, the pixels that exhibited high MF scores and low Infeasibility scores (Figure 5) to produce the final emergent sedge classification. Due to the spectral similarities in the vegetation present across the Cabin Creek floodplain, we were forced to select image pixels with a minimum MF threshold of 0.6.

Bighorn Crags Study Site

We were not able to identify any image endmembers that classified all water bodies (i.e., lakes, ponds, pools) well with the hyperspectral data, and consequently we classified standing water in the hyperspectral data using the same strategy described for delineating water in the Landsat ETM+ data. We loaded band 20 (0.727μm) vs. band 33 (0.9047μm), two near-infrared spectral bands, and selected all of the pixels that were located in the lower left corner paying close attention not to select non-water pixels (Figure 6). The 2-D scatter plot is interactively linked to the displayed image, and we focused on known areas of standing water (i.e., large ponds and lakes) to decide when the pixel selection began to overpredict non-target pixels.

We identified an Emergent Sedge (ES) endmember (Figure 7) located in the sedge dominated periphery of one of our training sites. This endmember was mapped and used as a proxy to help locate small emergent wetland sites and also wet meadow areas typically associated with amphibian foraging habitat in this study site. We used the MTMF algorithm to map sub-pixel abundances of the ES endmember. We loaded the MF and Infeasibility images as the axes of a 2-D scatter plot diagram and subjectively selected the pixels that exhibited high MF scores and low Infeasibility scores (Figure 8) to produce the final ES classification.

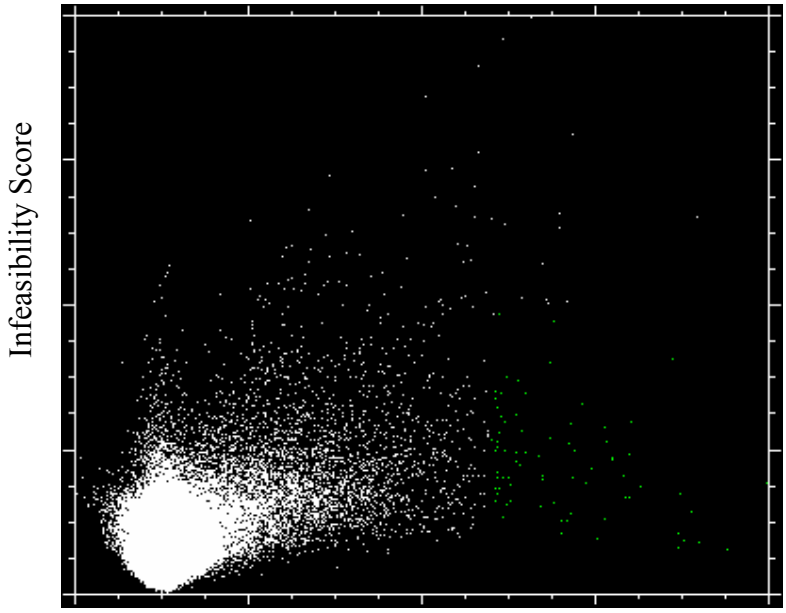

Figure 5. 2-D scatter plot of the Matched Filter and Infeasibility results from the MTMF classification algorithm applied to the wet meadow (WM) endmember. Final classified pixels are shown in green while the remaining background image pixels are shown in white.

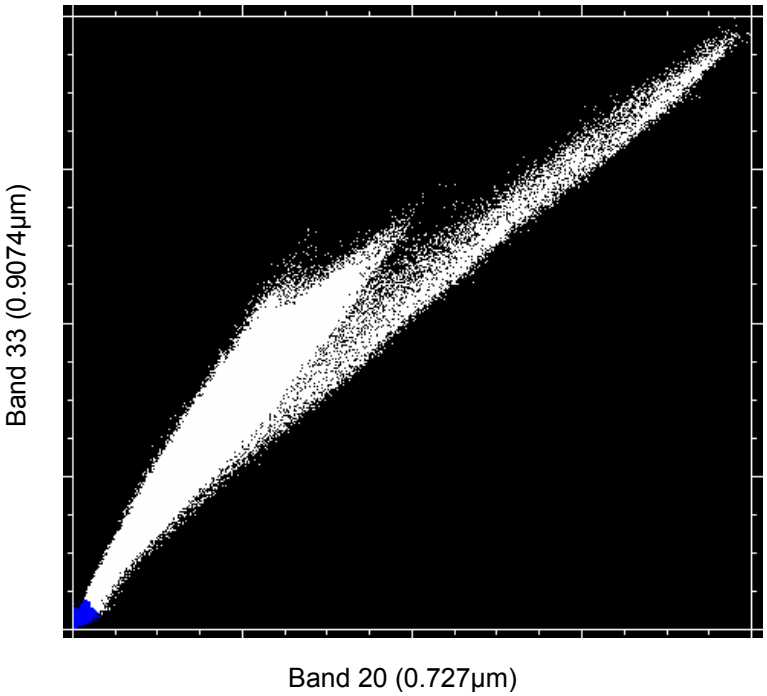

Figure 6. 2-D scatter plot showing the pixel selection used to create the standing water class. Final water pixels are shown in blue while all remaining image pixels are shown in white

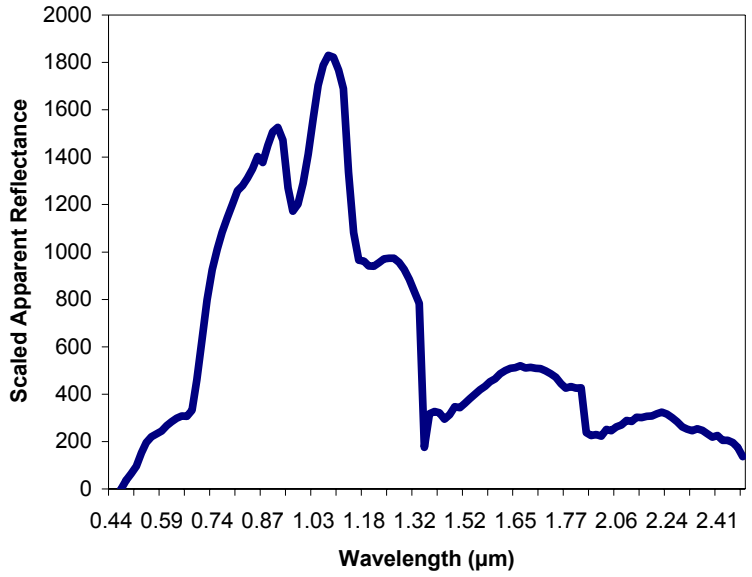

Figure 7. Emergent Sedge (ES) endmember spectral profile.

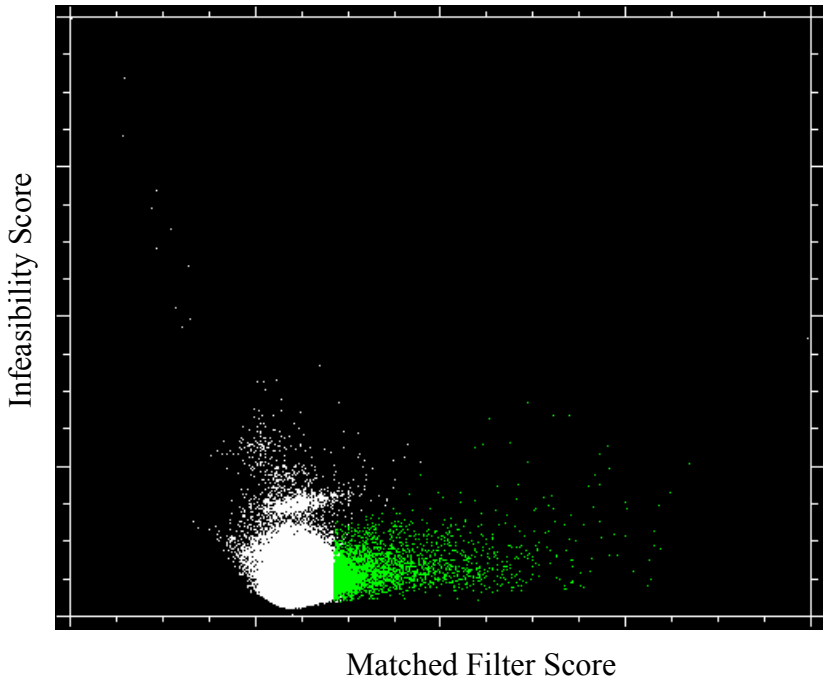

Figure 8. 2-D scatter plot of the Matched Filter and Infeasibility results from the MTMF classification algorithm applied to the emergent sedge endmember. Final classified pixels are shown in green while the remaining background image pixels are shown in white.

Accuracy Assessment

Error matrices serve as the basis for descriptive statistical techniques used to evaluate classification accuracy (Lillesand and Kiefer 1994, Congalton and Green 1999). Producer's accuracy is calculated by dividing the total number of correct pixels in a category by the total number of pixels actually identified from ground truth reference data (Congalton and Green 1999). Producer's accuracy represents the probability a true positive location on the ground is correctly classified. User's accuracy is calculated by dividing the total number of correctly classified pixels by the total number of pixels classified in that category (Congalton and Green 1999). User's accuracy represents the probability that a classified image pixel is actually that category on the ground (Story and Congalton 1986). Omission and commission errors are calculated by subtracting producer's and user's accuracy from 100% respectively.

Currently the ability to perform advanced image classifications has progressed in parallel to technological advances, but the corresponding ability to quantify accuracy has not followed this progression (Lillesand and Kiefer 1994). High spatial resolution data (i.e., 5m or less) commercially available from numerous sensors, challenges the capability of GPS receivers to accurately locate points on the ground when the topography is complex and canopy cover disrupts a clear view of the sky. Aside from the technical limitations of using GPS in many field study areas, image georeferencing procedures of airborne high spatial resolution data sometimes fail to provide highly accurate corrections. Even with a sophisticated GPS/IMU and ray tracing program recording X, Y, and Z coordinates for every image pixel (Boardman 1999), drastic fluctuations in ground elevation cause significant error in the georeferencing process. This means the coordinates of certain image pixels may be spatially skewed in a non-systematic direction, which makes locating individual pixels on the ground extremely difficult if not impossible. Similar to other validation studies involving high spatial resolution data (Aspinall 2002, Marcus 2002, Crabtree et al., *in press*), we used the classified imagery as a field map and navigated directly from it using obvious features (e.g., lake coves, stream bends, and rocky outcrops) as geographic references.

We chose to use groups or clusters of pixels as the sampling unit for the high spatial resolution (i.e., ADAR 5500 and HyMap) classification validation. The Landsat ETM+ spatial resolutions are within an expected positional range of accuracy common with current GPS receivers, which allowed us to consider individual pixels as a sampling unit. We did not want to exclude any sites large enough in spatial extent to fill a 30 m pixel, because many important wetland sites are much smaller than the spatial resolution of this imagery.

There are a number of suggestions published for developing a validation site selection scheme, each with their own advantages and disadvantages (Congalton 1991). Because the primary goal of this study was to identify wetland habitats that are low in abundance and widely dispersed throughout the scene, we felt the most appropriate validation was to visit all of the classified potential wetland sites. We walked the shorelines of lakes and visually searched meadows and backwater areas while in transit between predicted sites, and used previously collected field data from the study area (Charles R. Peterson, David

S. Pilliod, Crystal Strobl, and Jeremy P. Shive, unpublished data, Pilliod and Peterson 2001, Pilliod and Peterson 2002) as ground truth to evaluate omission errors.

CLASSIFICATION RESULTS AND DISCUSSION

Big Creek Study Site

The wetland locations within the Big Creek study site are a combination of primarily small ponds, wet meadows, and stream associated features such as pools and backwater channels. Many of the wet meadow sites have small ephemeral pools of water that were difficult to accurately detect. A total of 30 wetland sites exist within this study area based on past field surveys and newly located sites. Both multispectral datasets performed poorly at this study site while the hyperspectral data (combined) performed above average (Table 3).

Table 3. Accuracy assessment summary table for the Big Creek study site.

	Producer's Accuracy	User's Accuracy	Overall Accuracy	Omission Error	Commission Error
Landsat ETM+ (Water)	0%	0%	0%	100%	100%
ADAR 5500 (Water)	26.7%	72.7%	39.0%	73.3%	27.3%
HyMap (SWS)	43.3%	92.9%	59.1%	56.7%	7.1%
HyMap (SSW)	23.3%	100%	37.8%	76.7%	0%
HyMap (WM)	30.0%	56.3%	39.1%	70%	43.8%
HyMap (Combined)	83.3%	75.8%	79.4%	16.7%	24.2%

The Landsat ETM + water classification produced the poorest accuracy results possible for a remote sensing application with a producer's and user's accuracy of 0%. Even the largest pond within the study site (i.e., Bufo-Moose pond approximately 1400 m^2 in size) was not detected due to the large spatial resolution of the imagery. This site is a major source breeding pond for Western Toads (*Bufo boreas*) and Columbia Spotted Frogs (*Rana luteiventris*). The inability of this dataset to identify a single large wetland site questions the applicability of this imagery for inventory and monitoring efforts

Surprisingly the high spatial resolution of the ADAR 5500 data did not substantially contribute to a more successful classification of wetland habitat. The calculated producer's and user's accuracy were 26.7% and 72.7% respectively. Three wetland sites were falsely overpredicted and confused with the shadow class, while 73.3% (i.e., omission error) of the known wetland sites were missed. The ADAR 5500 imagery best identified stream associated features, such as side channels and pools, but did not identify wet meadows and small pool locations adequately. Our attempts to map an indicator variable, sedge, were not successful and consequently we were not able to accurately identify wet meadow features with the water class alone since the spectral response of these sites is dominated by vegetation presence. The single largest pond, Bufo-Moose

pond, was accurately identified while a smaller exposed pond located on the Cabin Creek floodplain was unexpectedly missed.

The HyMap hyperspectral data produced some of the highest classification accuracies for each individual endmember, and a combined accuracy that far exceeds the results from either multispectral dataset. The clear advantage of the hyperspectral data is the ability to identify multiple wetland features and indicator variables such as sedge presence to identify small sites. We calculated producer's and user's accuracy for the SWS endmember at 43.3% and 92.9% respectively. This endmember successfully identified most small ponds and pools while only slightly overpredicting one location in a forested riparian area.

The SSW endmember was used to complement the SWS classification by primarily identifying stream associated features, particularly side channels and backwater pools that we observed as late season Western Toad breeding sites in 2002. The producer's and user's accuracy for the SSW endmember were 23.3% and 100% respectively. These results illustrate the importance of considering multiple measures of classification accuracy. A user's accuracy of 100% (i.e., 0% commission error) simply means that every pixel that was classified as water in the scene is actually water on the ground. Reporting this result alone could mistakenly suggest an above average performance of this classification when in reality it performed poorly if the goal is to identify all wetland habitat in the study site.

The WM endmember was instrumental in identifying the wet meadow and ephemeral pool sites commonly missed by the other water related endmembers. The producer's and user's accuracy for the WM endmember were 30% and 56.3% respectively. The WM user's accuracy was the lowest reported at this study site illustrating the difficulty of accurately mapping this feature without overpredicting false positive sites. Even though 70% (i.e., omission error) of the total sites were missed, the true positive predicted sites located wet meadows that no other dataset was capable of predicting.

Individually, each HyMap endmember did not perform particularly well, but the utility of this imagery is that all of the features can be combined to produce one superior classification. We calculated a combined producer's accuracy of 83% (25/30) by summing all of the true positive locations among endmembers and divided by the total number of wetland sites. From an inventory and monitoring perspective the omission error is the most important measure of success while some overprediction (i.e., commission errors) is acceptable if the goal is identify all potential amphibian habitat in a study area.

From the standpoint of a herpetologist, the most significant result of the HyMap classification is identifying new sites that were not previously known from field surveys. We found a new backwater channel with breeding Western Toads and larval Columbia Spotted Frogs present. We discovered a second new backwater channel on the Cabin Creek floodplain that was not recognized through on the ground visual-assessment of the

area. We also identified a moderate sized forested pond representing a new potential breeding site with shallow water depths and an abundance of emergent vegetation.

Bighorn Crags Study Site

The Bighorn Crags study site is characterized by an abundance of high mountain lakes with forested pools and wet meadows dispersed throughout the landscape. A total of 48 wetland sites are present within this study site based on previous field surveys and one additional site identified through this research. The majority of wetland sites are lakes that on average are larger than the largest site in the Big Creek study site, and as a result the corresponding classification accuracies are much higher for all datasets (Table 4).

Table 4. Accuracy assessment summary table for the Bighorn Crags study site.

	Producer's Accuracy	User's Accuracy	Overall Accuracy	Omission Error	Commission Error
Landsat ETM+ (Water)	48.9%	100%	65.7%	51.1%	0%
ADAR 5500 (Water)	61.5%	100%	76.2%	38.5%	0%
HyMap (Water)	75%	94.7%	83.7%	25%	5.3%
HyMap (Sedge)	72.9%	89.7%	80.5%	27.1%	10.3%
HyMap (Combined)	91.7%	89.8%	90.7%	8.5%	10.2%

The Landsat ETM+ imagery produced the lowest classification accuracies with producer's and user's accuracy of 49% and 100% respectively. A producer's accuracy of 49% (i.e., 51% omission error) means that only half of the total true sites were actually identified. The predicted water sites were highly accurate with a commission error of 0%.

The wetland sites correctly identified consisted of large lakes and ponds while smaller ponds, emergent wetlands, and wet meadows were consistently missed likely due to their small spatial extent. Missed sites included the main source breeding location for Columbia Spotted Frogs, known as Frog Pond. A second crucial site completely missed was a smaller emergent wetland, named Axe Handle Meadow, that is the location of the only known Western Toad breeding site in the basin (David S. Pilliod, unpublished data).

The ADAR 5500 data produced slightly better results with producer's and user's accuracy of 61.5% and 100% respectively. The predicted wetland sites were again highly accurate (i.e., 0% commission error), but a number of small ponds and wet meadows were not identified and not reflected in this measure of accuracy. An omission error of 38.5% clearly depicts some limitations of this dataset, even when the wetland features are relatively large in size.

Frog Pond, the critically important Columbia Spotted Frog breeding site, was accurately identified while numerous wet meadows and forested ponds were missed. Axe Handle Meadow was missed again with this dataset and represents a significant error at a site

essential for understanding local Western Toad population status. The primary reason many of the wet meadow sites were missed is because we were not able to use an indicator variable, such as sedge presence, to assist in the identification of important wet and flooded meadow sites. Wet and/or flooded meadows are an important habitat type utilized by amphibian populations in the study area. These features are extremely difficult to predict using solely water features because the spectral response is highly influenced by vegetation presence. The limited number of spectral bands restricts the probability of correctly classifying these features, and imagery that provides an increased spectral range and spectral resolution will ultimately be needed to successfully model these types of wetland sites.

The Hymap hyperspectral data produced the highest classification accuracies of the datasets compared in this study. The water feature alone correctly classified more true positive sites than either multispectral datasets with producer's and user's accuracy of 75% and 94.7% respectively. Two sites were inaccurately overpredicted (i.e., 5.3% commission error) and confused with shadow. A total of 12 sites, which primarily consisted of wet meadows, were missed using this classification method.

The ES endmember yielded a slightly less accurate classification compared to the water feature with producer's and user's accuracy of 72.9% and 89.7% respectively. We evaluated the accuracy of this feature as a predictor of wetland presence and calculated accuracy based on ground truth data of all known wetland sites (i.e., a predicted sedge site was viewed as a predicted wetland site). This feature obviously did not correctly classify large deep lakes that lacked shallow shorelines with sedge present, but was extremely effective at identifying wet meadows and ephemeral pools missed by all other classified features and datasets. We assessed the accuracy of this feature explicitly (i.e., a predicted sedge site was evaluated as sedge and not a wetland) to assess how well the sedge classification actually performed at predicting sedge presence. We visited a total of 57 predicted sedge sites and calculated a producer's and user's accuracy of 98.3% and 91.8% respectively. Clearly the high accuracy of this feature supports future considerations to use sedge presence as a predictor variable for wetland presence, at least in the regions of the western U.S. where sedge presence is highly correlated to wetland and amphibian presence.

Although both the water feature and ES endmember produced higher accuracies than the multispectral datasets, the real advantage of the hyperspectral data is the capability to combine individual feature results for unparalleled accuracy results. We added all of the true positive predictions and divided by the total number of wetland sites present in the study site to calculate a combined producer's accuracy of 91.7% (44/48). All overpredicted sites that led to non-wetland locations were added to calculate a combined user's accuracy of 89.8%. This level of accuracy provides a near comprehensive prediction of all wetland sites present within the study site providing the detailed information necessary for effective inventory and monitoring programs.

One of the most significant results from the HyMap classification is the discovery of a new forested pond. We have a thorough and detailed understanding of the wetland

habitat available in this study site as a result of ongoing long term repeated survey (David Pilliod unpublished data). In fact, other than a single new pond discovered this summer every other wetland location was previously identified and surveyed. No amphibians were observed at this new site, but the characteristics of the pond (e.g., fishless) suggest that amphibians may utilize this location sometime during their active season.

Comparison against Traditional Methods

For a comparison to traditional site selection processes we used USGS 7.5 minute topographic (Topo) maps and DOQQ's to identify all wetland sites labeled on the map or clearly visible in the aerial photographs (Figures 9 and 10). The DOQQ's used in this study are black-and-white, but color DOQQ's are becoming available in many areas providing a more useful dataset for identifying wetland habitat. The Landsat ETM+ classification produced fewer true positive sites than the total recognized from Topo maps and DOQQ's (note: no DOQQ's exist over the Bighorn Crags study site). Across our study area, more wetlands would be accurately located if we used traditional sources instead of expending effort to classify the Landsat ETM+ imagery.

The ADAR 5500 data successfully identified more wetland sites than traditional Topo maps, but slightly less than the DOQQ's in the Big Creek study site (Figures 9 and 10). The combined processing time required to georeference the imagery and classify the ADAR 5500 data far exceeds the total amount of time needed to visually interpret DOQQ's. The greatest limitation of these data is the inability to accurately identify indicator variables, such as sedge presence, that can be used as a proxy for predicting wetland distributions.

The HyMap hyperspectral data clearly produced the greatest accuracies while providing a fine-scale level of information instrumental in understanding amphibian habitat distributions in the study area. Each individual endmember did not produce classification accuracies significantly better than the other datasets in this study excluding Landsat ETM+ (Figures 9 and 10). However, when all of the endmember accuracies are combined, this dataset yields the greatest accuracies accomplished in this study.

Assessment of Error and Bias

We performed all image classification efforts following a preliminary site survey and ground training data campaign. In addition, our background knowledge of the study area compiled through multiple years of previous field based surveys provides an informed perspective of the current amphibian habitat distributions. We made a number of subjective decisions concerning classification thresholds, training data pixel selection, and decisions on the final "best" classification map. These decisions are influenced by our familiarity with the study area and would expectedly differ from a classification effort performed with no background knowledge of the study area. Typically prior to inventory surveys little or no detailed background information is available for a study area potentially complicating the effort required to create a comparably accurate classification. It would be beneficial to repeat this study in an

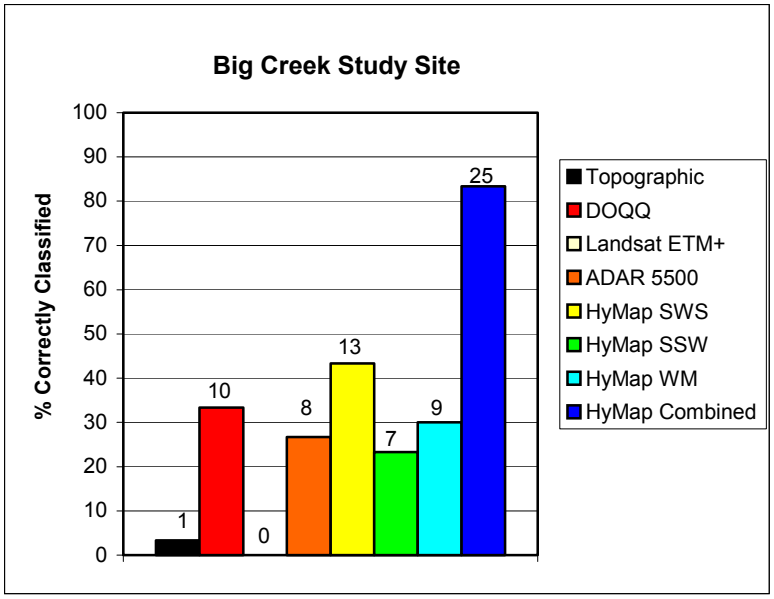

Figure 9. A comparison of correctly classified sites resulting from different data sources. The numbers above each dataset represents the total number of true positive sites predicted by each classified dataset of the 30 total wetland sites present in the Big Creek study site.

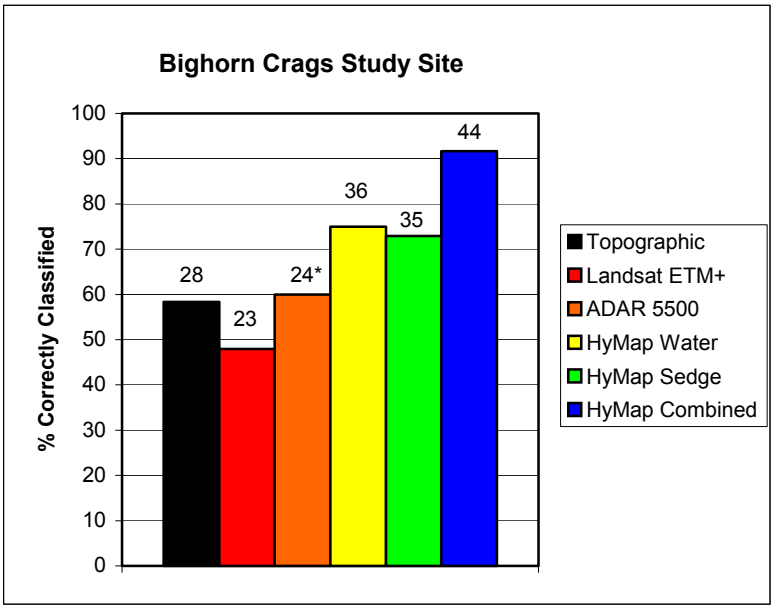

Figure 10. A comparison of correctly classified sites resulting from different data sources. The numbers above each dataset represents the total number of true positive sites predicted by each classified dataset of the 48 total wetland sites present in the Bighorn Crags study site. (* note: the ADAR 5500 coverage did not extend over the entire Bighorn Crags study site and consequently the total number of wetlands sites was reduced to 40)

unfamiliar region and compare the results to determine widespread application in inventory and monitoring programs.

We chose to navigate to all predicted sites using the final classification map as a reference opposed to using GPS and navigating using site coordinates. The high spatial resolution of the ADAR 5500 and HyMap imagery require coordinate accuracies consistently within 5 m of absolute true ground position. Without real-time differential correction capabilities, GPS coordinates collected in a region with rugged topography and forest canopy will rarely be accurate to within 5 m of absolute error. The georeferencing process contributes additional errors to image pixel coordinates and further lowers the probability of confidently locating individual pixels in the field. Until GPS accuracies increase and georeferencing algorithms advance, the assessment of high spatial resolution imagery will remain difficult and influenced by error.

Costs of Imagery

The total cost of each remotely sensed dataset needs to be evaluated if these technologies are going to be considered or actually become incorporated into inventory and monitoring programs typically constrained by funding. The financial reality of many long-term research initiatives limits the possibility of incorporating expensive technology that may only perform marginally better than a less expensive approach. A cost comparison of the imagery provides a perspective to consider accuracy and knowledge gained from a financial perspective.

Satellite based data will normally cost less than airborne imagery because many of the mobilization costs and acquisition logistics are no longer a substantial consideration. The Landsat ETM+ data was the most inexpensive data set acquired, regardless of the unfortunate geographic location of the study area that spans two adjacent Landsat scenes boundaries. A Landsat scene costs $600 for a Level 1G radiometrically and geometrically corrected dataset with each additional scene offered at a reduced rate of $250 (http://edcdaac.usgs.gov/pricing_policy.html). Considering the additional handling fee of $5, the total cost of the Landsat ETM+ data was $855 (Table 5).

The ADAR 5500 dataset is the second most expensive imagery collected and has a number of acquisition fees and financial considerations associated with a specific contracted collection. Many of the costs we are reporting reflect the logistical considerations for the contracted data collection of this project, and the costs may be variable depending on a different contract and extent of data collection. Mobilization fees that cover the estimated number of images contracted, and the corresponding estimated number of flight and standby days required, adds to a total of $4000. The image acquisition fees for the total area contracted in this data collection cost $11500, and includes expenses for flight operations engineer, insurance, and associated costs for the data capture. It is important to note that the contracted data collection covered a much larger spatial extent than this study area alone, and much of the data collected were not used for our research. This would lower this category total but it is hard to estimate how much cost would appropriately be deducted, so we approximated a cost of about 2/3

the total equaling $7660. There are also post capture processing fees of $2000 for vignetting corrections and band-to-band coregistration for all images.

The ADAR data are collected as overlapping frames imposing a large amount of processing time needed to georeference and mosaic the scenes into one image. Positive Systems, Inc. offers the DIME software package that is designed specifically for georeferencing and mosaicking ADAR 5500 data and costs $1700 for the site registration and on-site training. There are 25 free processing credits provided with the site license, but additional costs of "image credits" for $5 each are needed to process and save output images. We could not use this program for the Bighorn Crags study site (i.e., DOQQ's are required as a basemap layer), so we did not consider any additional image credit costs because they were not needed for our research. These additional costs are mentioned as considerations for larger studies incorporating this data type. Adding up all of acquisition expenses sums to a total of $15360 for the entire study area (Table 5).

The HyMap hyperspectral data was the most expensive dataset collected over the study area. HyMap data are priced on a per flightline basis of $6000, and included in these costs are image post processing services such as atmospheric and geometric corrections. We collected one flightline of hyperspectral data over the Bighorn Crags study area and two flightlines over the Big Creek study area creating a total cost of $18000 (Table 5). It is important to note that the Big Creek study area could have been covered in a single flightline if appropriately planned, and this would have reduced the total number of flightlines dropping HyMap behind the ADAR 5500 sensor in total costs. The reported costs reflect the value at the time of our data acquisition and have since lowered in price with cost reduction incentives for larger data collects.

Table 5. A comparison of imagery costs.

Sensor	Costs
Landsat ETM+	
Single Scene	600
(x2 w/ reduced cost)	250
Handling Charge	5
	$855
ADAR 5500	
Mobilization*	4000
Image Acquisition*	7660
Post Capture Processing*	2000
DIME Software	1700
	$15,360
HyMap	
Single Flightline*	6000
(x3)	18000
	$18,000

* Reported costs are variable

Processing Time

This category is an additionally important consideration that must be evaluated when suggesting the most appropriate imagery for amphibian inventory and monitoring initiatives. Total processing time is very difficult to evaluate because we expect considerable variability in the length of time needed for different people to perform the same processing steps. This will certainly influence the amount of time and effort needed to accomplish the necessary image processing steps. We provide a summary of the time we expended to process and classify each dataset.

We made some background assumptions while assessing the total processing time that can be compared between analysts. First, we assumed that an image analyst is already trained in traditional remote sensing principles, processing, and applications, and we did not account for learning time except when necessary (i.e., hyperspectral image processing). Secondly we also impose a requirement, as part of the preliminary processing step, 7 days or 56 hours of ground training data collection and/or ground reconnaissance at each study site to become familiar with the study area prior to any image processing effort.

The Landsat ETM+ data took the least amount of time to process and classify. The data were provided already mosaicked and the remaining image processing time consisted of converting the DN values to at-sensor reflectance. We estimated this step to take about 2 days, or 16 hours. The image classification process includes time for ROI training class selection and refining, and experimental testing of classification algorithm applications that we estimated to total 10 days, or 80 hours. Including the initial ground truth campaign, total time expenditure results in 19 days, or 152 hours, to fully process and classify the Landsat ETM+ data (Table 6).

The ADAR 5500 data took the second greatest amount of time to process and was almost identical to the amount of effort expended on the Landsat multispectral dataset. The DIME software training took 2 days, or 16 hours, to complete in which time the Big Creek scenes were georeferenced and mosaicked. We spent an additional day, or 8 hours, attempting to manually mosaic the Bighorn Crags images before deciding to leave them in the raw format due to undesirable results. Similar to the Landsat data, we estimated 10 days, or 80 hours, for image classification time including ROI selection and the testing numerous classification algorithms. Including the time needed for the ground truth campaign, the total estimated processing time for the ADAR 5500 data was 20 days or 160 hours (Table 6).

The HyMap hyperspectral data unquestionably took the greatest amount of time to process and classify attributed to the total time of learning the specifics of hyperspectral data analysis techniques and applications. Many of the common hyperspectral image processing steps are unique to this data type, and are not encountered working with multispectral data. We attended an hyperspectral training short-course that occurred over 5 days, or 40 hours, which formed the foundation of our knowledge of hyperspectral analyses. We suggest this training as a precursor for correctly and effectively processing

hyperspectral data, and consider this training part of the processing effort that should be included. We estimate the georeferencing procedures lasted 10 days, or 80 hours, with the majority of the time attributed to learning the correct processing steps specific to hyperspectral data and understanding various results. We performed data reduction techniques, such as the MNF transform, PPI, and the n-D Visualizer which lasted 15 days, or 120 hours, with much of the processing time a result of redundant testing of processing steps to better understand intermediate results. Finally, we estimate the image classification procedure took a total of 10 days, or 80 hours of time to complete with many repetitive steps interpreting the results and refining the input parameters. This results in a total of 47 days, or 376 hours, to complete the hyperspectral data analyses (Table 6).

Table 6. A comparison of categorized image processing times and associated time.

Sensor	Processing Step	Time (days)	Time (hours)
Landsat ETM+	Ground Training	7	56
	Reflectance Conversion	2	16
	Image Classification	10	80
		19	**152**
ADAR 5500	Ground Training	7	56
	Georeferencing/Mosaic	3	24
	Image Classification	10	80
		20	**160**
HyMap	Ground Training	7	56
	Hyperspectral Training	5	40
	Georeferencing	10	80
	Data Reduction	15	120
	Image Classification	10	80
		47	**376**

CONCLUSIONS

Illustrated through this comparative application and assessment, it is clearly recognized that different scales of remotely sensed data will produce varying accuracy results within the same study area. From an inventory and monitoring perspective, the dataset that provides the most cost-effective and comprehensive habitat information is the most desired. Our results provide insight into the relative performance of three vastly different dataset for predicting amphibian habitat and we offer some suggestions for further evaluation and future inventory and monitoring applications.

The Landsat ETM+ sensor has traditionally been viewed as a valid resource for numerous natural resource applications due to the consistency and availability of data. For some applications (e.g., forest fragmentation studies) the 30 m spatial resolution of this dataset may be appropriate because the scale of observation correctly corresponds to the scale of processes governing the feature of interest. Unfortunately many wetland sites most important for amphibians are typically not large lakes but smaller isolated ponds less than

30 m^2 in area. The results from both study sites reveal a significant limitation of this imagery for accurate identification of wetland habitat regardless of the inexpensive costs of these data.

The ADAR 5500 data performed below expected levels of accuracy even though this imagery exhibits the highest spatial resolution compared in this study. Given the fact that many of the wetland sites within the study are small in spatial extent, this dataset would expectedly classify these locations most accurately. We feel that the limited number of spectral bands contributed to the difficulties of distinguishing water features from other spectral classes such as shadow. The ADAR 5500 sensor collects only a single band in the near-infrared spectral wavelengths. We found that the near-infrared region was paramount in providing spectral information necessary for delineating water from other features, and because these data lack multiple near-infrared spectral bands, classifying water features was more difficult.

Aside from considering the accuracy statistics, potentially the most important result from the HyMap image classification is that new previously unknown wetland sites were discovered in areas that have been repeatedly surveyed on the ground. These results are similar to another study in Yellowstone National Park where new amphibian breeding sites were located in unexpected areas (Crabtree et al., *in press*). The ultimate goal of an inventory program is to comprehensively survey all available habitats within a study area, and the HyMap hyperspectral data exhibit the best potential for accomplishing this goal by providing near comprehensive identification of wetland habitat within the study area. The goal of monitoring programs is to understand how particular habitat features are changing over time. Given the ability to map fine scale wetland features, we can begin to subdivide predicted habitat into specific types of amphibian habitat such as breeding, foraging, and overwintering. These wetland features can be used as a surrogate to infer changing population status and habitat conditions across large landscapes. By identifying particular habitat features, such as the abundance of emergent sedge, we can begin to extrapolate distribution and occurrence predictions to other areas were there are no field data.

The hyperspectral data certainly have the capability to be successfully incorporated into inventory and monitoring programs, but warrants additional research to assess repeatability and application in diverse environmental landscapes. One immediate limitation would be the large cost and processing time associated with collecting hyperspectral imagery over large spatial extents. Costs have already begun to drop since we started this research and will expectedly continue to decrease as this technology becomes more common. Hyperspectral imagery should be considered a valuable tool for future inventory and monitoring programs with new potential applications yet to be explored.

ACKNOWLEDGEMENTS
This study was made possible by a grant from the National Aeronautics and Space Administration Goddard Space Flight Center. ISU would like to acknowledge the Idaho Delegation for their assistance in obtaining this grant. We would also like to thank Jim and Holly Akenson of the Taylor Ranch Research Station for their hospitality and logistical support during our visit to the Big Creek study site. We would also like to thank David Pilliod for all of his support, assistance, and suggestions with the Bighorn Crags study area.

LITERATURE CITED

Aspinall, R.J. 2002. Use of logistic regression for validation of maps of the spatial distribution of vegetation species derived from high spatial resolution hyperspectral remotely sensed data. Ecological Modelling 157: 301-312.

Boardman, J.W. 1993. Automated spectral unmixing of AVIRIS data using convex geometry concepts. *Summaries, 4th JPL Airborne Geoscience Workshop*, JPL Publication 93-26(1): 11-14

Boardman, J.W. 1998a. Post-ATREM polishing of AVIRIS apparent reflectance data since EFFORT: a lesson in accuracy versus precision. Proceedings of the 7th JPL Airborne Earth Science Workshop. JPL Publication 97-21(1): 53.

Boardman, J.W. 1998b. Leveraging the high dimensionality of AVIRIS data for improved sub-pixel target unmixing and rejection of false positives: Mixture Tuned Matched Filtering. AVIRIS 1998 Proceedings, Jet Propulsion Laboratory, Pasadena, Ca. 6.

Boardman, J.W. 1999. Precision geocoding of low altitude AVIRIS data: lessons learned in 1998. *AVIRIS 1999 Proceedings*, Jet Propulsions Laboratory, Pasadena, Ca. 6.

Boardman, J.W., F.A. Kruse, and R.O. Green. 1995. Mapping target signatures via partial unmixing of AVIRIS data. *Summaries, 5th JPL Airborne Earth Science Workshop*, JPL Publication 95-1: 23-26.

Cocks, T., R. Jenssen, A. Stewart, I. Wilson and T. Shields. 1998. The HyMap airborne hyperspectral sensor: the system, calibration and performance. Presented at the 1st EARSEL Workshop on Imaging Spectroscopy, Zurich, Switzerland.

Congalton, R.G. 1991. A review of assessing the accuracy of classifications of remotely sensed data. Remote Sensing of Environment 37: 35-46.

Congalton, R.G., and K. Green. 1999. *Assessing the Accuracy of Remotely Sensed Data: Principles and Practices*. CRC Press Inc., Boca Raton, Florida.

Crabtree, R.L., W.A. Marcus, K.Q. Halligan , J.W. Boardman, J.E. Norland, M. Mirik, C.R. Peterson, and R. Cooper. *In Press*. High Resolution Hyperspectral data for remote measurement of ecological variables: Evaluation and applications. Photogrammetric Engineering and Remote Sensing.

Duffie, J.A., and W.A. Beckman. 1980. Solar Engineering of Thermal Processes. John Wiley and Sons, New York. p.109.

Fellers, G.M. 1997. Design of amphibian surveys. In, D.H. Olson, W.P. Leonard, and R.B. Bury (eds). *Sampling Amphibians in Lentic Habitats*. Society for Northwestern Vertebrate Biology: 23-24.

Gao, B.C., K.B. Heidebrecht, and A.F.H. Goetz. 1993. Derivation of scaled surface reflectances from AVIRIS data. *Remote Sensing of Environment* 44: 165-173.

Gao, B.C., K.B. Heidebrecht, and A.F.H. Goetz. 1997. Atmosphere removal program (ATREM) Version 3.0 user's guide. Center for the Study of Earth from Space, University of Colorado, Boulder. 1-27.

Green, A.A., M. Berman, P. Switzer and M.D. Craig. 1988. A transform for ordering multispectral data in terms of image quality with implications for noise removal. IEEE Trans. Geosci. Remote Sens. Vol. 26(1): 65-74.

Harsanyi, J.C. and C.I. Chang. 1994. Hyperspectral image classification and dimensionality reduction: An orthogonal subspace projection approach. *IEEE Transactions on Geoscience and Remote Sensing* 32: 779-785.

Jensen, J.R. 2000. *Remote Sensing of the Environment, An Earth Resource Perspective*. Prentice Hall, Upper Saddle River, New Jersey.

Kruse, F.A., A.B. Lefkoff, J.B. Boardman, K.B. Heidebrecht, A.T. Shapiro, P.J. Barloon, and A.F.H. Goetz. 1993. The spectral image processing system (SIPS)-Interactive visualization and analysis of imaging spectrometer data. Remote Sensing of Environment 44: 145-163.

Lillesand, T.M., and R.W. Kiefer. 1994. *Remote Sensing and Image Interpretation*, 3rd Edition. Wiley, New York.

Marcus, W.A. 2002. Mapping of stream microhabitats with high spatial resolution hyperspectral imagery. Journal of Geographic Systems 4: 113-126.

Pilliod, D.S. and C.R. Peterson. 2001. Local and landscape effects of introduced trout on amphibians in historically fishless watersheds. Ecosystems 4: 322-333.

Pilliod, D.S., and C.R. Peterson. 2002. Evaluating effects of fish stocking on amphiban populations in wilderness lakes. In: Cole, D.N., S.F. McCool, W.T. Borrie, and J. O'Loughlin editors. Wilderness science in a time of change conference. Volume 5, Wilderness ecosystems, threats, and management. Proceedings RMRS-P-15-Vol-5. Ogden (UT): USDA Forest Service, Rocky Mountain Research Station. p 328-335.

Richards, J.A. 1999. Remote sensing digital image analysis. Springer-Verlag, Berlin. 240.

Research Systems, Inc. 2002. Environment for Visualizing Images User's Guide Version 3.5, Boulder, Colorado.

Story, M., and R. Congalton. 1986. Accuracy assessment: A user's perspective. Photogrammetric Engineering and Remote Sensing 52(3): 397-399.